ADVANCES IN LASER FORMING RESEARCH

Y. Lawrence Yao, Peng Cheng, Duncan Pratt and Yajun Fan
Department of Mechanical Engineering, Columbia University, USA

Abstract: In this review, a number of recent developments of laser forming are presented based on the work in Manufacturing Research Laboratory (MRL) of Columbia University**.** In order to advance laser forming to realistic forming application, it is necessary to consider non-straightening and larger scale 3D laser forming, so that anisotropy and size effect need to be investigated in detail. In this paper, the textures of cold-rolled mild steel sheets are characterized and the influence of plastic anisotropy on laser forming process is investigated. Deformation textures are measured in terms of pole figures and orientation distribution function (ODF) plots obtained through electron backscatter diffraction (EBSD). Effects of plastic anisotropy on laser forming process under various conditions, such as different laser power, scanning speed, number of scans for sheets of different rolling reductions are experimentally and numerically investigated. In present paper, the influence of size effect, including variation of sheet width and sheet length, on laser -induced deformation is also investigated. Distinctive trends in bending angle are identified for varying sheet width, length or both. The results are interpreted in terms of heat sink effect and bending non-uniformity. An analytic model is developed to facilitate size effect prediction. The model is based on the solution to a moving strip heat source over a finite size sheet and on the account for pre-bending effect among consecutive segments on the scanning path. Analytical results are compared with an existing analytical model and numerical simulation.
Keywords: *Laser forming, Sheet metal, Anisotropy, Size effect*

1. Introduction

Laser forming is a flexible forming process that forms sheet metal by means of stresses induced by external heat instead of external force. Understanding various aspects of laser forming has been a challenging problem of considerable theoretical and practical interest. There has been a lot of work carried out on two-dimensional laser forming. However, in order to advance the process further for realistic forming application, it is necessary to consider non-straightening and larger scale 3D laser forming. In such case, anisotropy and size effect in laser forming need to be investigated in detail.

Anisotropy includes elastic and plastic anisotropy. In cold rolled sheet, elastic deformation is much smaller compared with the plastic deformation, so only the anisotropic plasticity is normally considered [1]. The type of plastic anisotropy usually desired in sheet metal forming is that in which the sheet is isotropic in the plane and has an increased strength in the thickness direction, which is normally referred to as normal anisotropy. More often, however, the type of plastic anisotropy is characterized by different strengths in different directions in the plane of the sheet, which is called planar anisotropy. This is simply because of the different amount of deformation along the rolling and other directions in the plane. The plastic anisotropy is commonly characterized by *R*-values, which will be explained in more details in late sections. In this study, the planar plastic anisotropy is simply referred to as anisotropy. The primary source of such plastic anisotropy comes from the texture or the preferred crystallographic orientations of the grains as a result of cold rolling. The plastic anisotropic properties of sheet metals have generally been investigated independently by two approaches [2]. The first one is to develop various macroscopic yield functions from a phenomenological viewpoint. The second approach is to develop polycrystal models based on the constitutive behavior of crystalline slip in single crystals.

In present study, the effect of anisotropy exhibited in cold-rolled mild steel on laser forming process is investigated. To better characterize the anisotropy, pole figures and ODF plots of steel sheet were obtained by EBSD and compared with those predicted by deformation texture theories. *R*-values were measured and compared with those predicted by theories. Effect of such anisotropy on laser forming under various conditions, such as different sheet thickness reductions, scanning speed, laser power as well as multiple scanning were investigated.

Geometric effect plays an important role in laser forming, however, most studies focused on the effect of workpiece thickness without considering other geometric attributes. Scully[3] proposed that plate thickness s_0 is one of the primary factors in laser forming and he adopted a quantity $P/(s_0\sqrt{V})$ that was used in arc welding to study the effect of plate thickness on bending angle, but he did not give an exact relationship between them. Koloman and Karol[4] proposed an analytical model in which the bending angle is a function of the reciprocal of the square of thickness. However, the bending angles calculated from this formula are some orders of magnitude too large

compared with experiments. Vollertsen[5,6] proposed a simple two-layer model based on the temperature gradient mechanism (TGM) assumption. Due to the assumption that bending deformation is uniform along the sheet length, the only geometric factor appeared in those models is plate thickness.

Experimental investigations and numerical simulation, however, have shown that sheet size has an effect on laser forming. Vollertsen pointed out that the width of the sheet influences the cooling conditions and therefore the bending angle, and he also observed the influence of the sheet length on stress state. But he did not consider the size influences in his analytical solutions. Hsiao[7] has found that for Inconel 625 the angular distortion increases as sheet length increases and he proposed the reason is the longer plate provides more cold metal to produce thermal stresses. He also proposed that there is an upper limit in the angular distortion with respect to the sheet length. However, these investigations on size effect are empirical and did not lead to analytical prediction.

In this paper, the experimental and numerical investigations aimed at advancing the understanding of the causes of the size effect in the straight-line laser forming are presented for a wide range of sheet sizes. Various deformation patterns due to the size effect are explained. To better quantify the role of size effect on laser forming, a predictive model is developed, in which finite sheet width and length are considered. The proposed model is experimentally validated.

2. Anisotropic effect on laser forming

2.1. Background

2.1.1. Deformation textures in BCC sheet metals

Sheet texture is described by the Miller index notation $(hkl)[uvw]$, in which the crystallographic plane (hkl) is roughly parallel to the sheet surface, and the direction [uvw] in that plane is roughly parallel to the rolling direction (*RD*). Various types of textures are possible to form in cold rolled sheet metal depending on material type and processing condition. Both experimental and simulation results have shown that four texture components, {001}<110>, {112}<110>, {111}<112> and {111}<110>, are possible in cold rolled *BCC* metals of initially random textures[8]. Which texture components in *BCC* metals are present and more dominant also depends on process condition[9]. For instance, when rolling reduction is moderate, (i.e. < 70%), {001}<110> and {112}<110> are the dominant components on the α-fiber, that is, <110> is parallel along *RD*, and one sees a weak preference of {111}<112> on the γ-fiber, that is, {111} is parallel along the normal direction (*ND*) of the sheet. For large rolling reduction (i.e. > 70%) the maximum on the α-fiber is shifted to {112}<110> and that on the γ-fiber from {111}<112> to {111}<110>.

The texture type developed in plastic deformation of polycrystals is usually controlled by crystallographic slip in the individual grains. It is the result of rotation of slip systems in grains during plastic deformation. Such rotations are along particular directions. For instance, in case of tension, the slip direction vector rotates gradually towards the tensile direction and the slip plane normal rotates away from the tensile axis. This characteristic orientation change is the major reason of rolling texture development and can be explained by Schmid and Taylor theory[10]. That is, in the tensile case, during the decrease of the angle between the tensile axis and slip direction, the Schmid factor decrease until another slip system with higher Schmid factor is activated instead. Then the slip direction of that newly activated slip system rotates towards the tensile axis. This process ends when it reaches a stable orientation. For the tensile case, [112] and [110] are the main stable orientations for *FCC* and *BCC* metals, respectively. Due to the multiple systems of slip for the *BCC* metals, there are multiple stable orientations. This also explains why multiple components of texture occur in *BCC* metals.

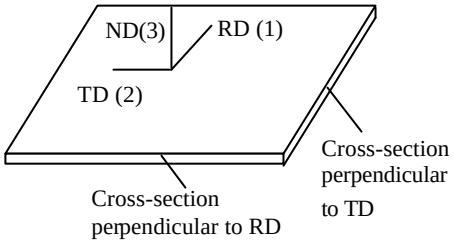

(a)

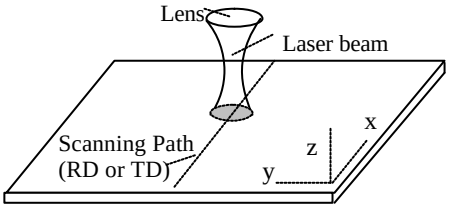

(b)

Fig.1 (a) Rolled-sheet coordinate system and terminology: *RD*: rolling direction, *TD*: transverse direction; *ND*: normal direction. (b) Schematic laser forming system scanning path along *RD* or *TD*.

2.1.2. Theoretical method to predict texture formation

To quantitatively predict the development of textures, several models were developed. The most widely applied model to predict the texture development is Taylor-like model[11], which assumes that the strain of individual crystallite is equal to the strain of the polycrystalline aggregate and is therefore called the " Full Constraint" (FC) model. Another assumption of the FC model is the

activation of at least five slip systems in each crystallite so that all five independent components of a general strain tensor may be accommodated. In Taylor's model, the work increment done during the tension process in terms of the macroscopic stress s_p and the strain increments de equals to the internal work done by the critical shear stress $t_0^{(r)}$ and shear strain increments $dg^{(r)}$ in the *r*-th slip system (r=1,2,..5).

$$s_p de = \sum_{r=1}^{5} t_0^{(r)} dg^{(r)} \quad (1)$$

Assuming the critical shear stress $t_0^{(r)}$ is the same for all slip systems and equal to t_0. The Taylor factor can be defined as

$$M = \frac{s_p}{t_0} = \frac{\sum_{r=1}^{5} dg^{(r)}}{de} \quad (2)$$

Taylor factor M can be compared with the reciprocal of the Schmid factor. Combinations of slip systems with the minimum Taylor's factor will be the active slip systems in the plastic deformation.

Deformation textures calculated according to the Taylor model are in fairly good qualitative agreement with the observed ones. However, some discrepancies exist when it was applied in large reduction cases. " Relaxed Constraint" (RC) models were developed based on the Taylor model to describe texture development in large deformation. Unlike the Taylor approach where strain compatibility is strictly prescribed, in the RC models partial constraints are imposed on the basis of mixed boundary conditions: some components of strain and the others of stress are presumed given. For cold rolling with large reduction, the RC models are more accurate to predict the texture development compared with the FC model. Two kinds of RC models were applied: one is the lath model with e_{13} relaxed, and the other is the pancake model with both e_{13} and e_{23} relaxed, where 1 represents the rolling, 2 the transverse, and 3 the normal direction (Fig. 1a). Kocks, et al. [8] pointed out that for simulating low reductions, the FC Taylor model is preferred. For describing intermediate reductions, the lath model, and for large reductions, the pancake model is more suitable.

2.2. Experimental and Simulation Conditions

2.2.1. Texture measurement

Texture measurements of AISI 1010 cold rolled steel sheets 1.4mm and 0.89mm thick were carried out using electron back-scatter diffraction (EBSD). A series of typical scans were recorded with a step size of $3mm$ and consisted of 3000-6000 indexed points. Four incomplete pole figures {100}, {110}, {111} and {112} were measured in the rolling plane (*RD-TD* plane where *TD* stands for transverse direction). Three-dimensional orientation distribution functions (ODFs) $f(g)$ were calculated by using the spherical harmonics. The ODFs are represented in three-dimensional Euler space in the range of $0^0 \le j_1, f, j_2 \le 90^0$ by way of iso-intensity contour lines in different sections with an Euler angle held constant. Grain structures in different cross-sections were observed by scanning electron microscope (SEM). Samples were polished and etched using 3% HNO_3 for 5 seconds for EBSD and 20 seconds for SEM.

2.2.2. Measurement of R-values

In accordance with the ASTM Standard E517, *R*-values of AISI 1010 cold rolled steel sheets 1.4mm and 0.89mm thick, were measured by uniaxial tensile test on a material testing machine. The specimens were cut by a CNC machine with axes along the rolling direction (*RD*), transverse direction (*TD*) and 45^o to the rolling direction, corresponding the measurement of R_0, R_{45} and R_{90}, where the subscripts represent the angle to the rolling direction.

The specimen has gage length of 1.6" and width of 0.4". Due to the difficulty in measuring gage thickness changes with sufficient precision, an equivalent relationship is commonly used, based on length and width strain measurements:

$$R = \frac{e_w}{e_t} = \frac{\ln(w_i / w_f)}{\ln(l_f w_f / l_i w_i)} \quad (3)$$

where e_w and e_t are true strain in width and thickness directions; w_i, w_f and l_i, l_f are initial and final gage width and length, respectively.

Measurement accuracy is improved as the strain is increased but within the necking limits. Strains of 10-20% are commonly utilized in determining the *R*-value of low carbon steels. In present study, approximate 15% plastic strain is utilized. The strain rate in the uniaxial tensile tests was taken to be 1.25×10^{-3}/s, which is within the range of the ASTM Standard ($<8.33\times10^{-3}$ /s).

2.2.3. Laser forming experiments

The material is cold-rolled AISI 1010 steel, and the workpiece size is 80 mm by 80 mm with thickness of 1.4 mm and 0.89 mm. Experiments of straight-line laser forming were carried out along *RD* and *TD*, respectively (Fig. 1b). The laser system used in the experiments is a PRC-1500 CO_2 laser, with a maximum output power of 1.5KW and power density distribution was TEM_{00}. In present study, various conditions such as different material reduction (corresponding to two different workpiece thickness levels), different scanning speed (from 50 mm/s to 90 mm/s), different laser power (from 600 w to 800 w) and number of scans (1 to 10) were applied. Laser beam diameter varied from 6 mm to 4 mm when the sample thickness changed from 1.4 mm to 0.89 mm. A coordinate measuring machine (CMM) is used to measure the bending angle at different positions along the scanning path. To enhance laser absorption by the workpiece, graphite coating is applied to the surface exposed to the laser.

2.2.4 Numerical simulation

In numerical simulation the laser forming process is modeled as a sequentially coupled thermal-mechanical process. In the thermal analysis, the transient conduction for a solid workpiece irradiated by a laser beam can be expressed in terms of temperature as:

$$r c_p \frac{\partial T}{\partial t} = \nabla \cdot (k \nabla T) \tag{4}$$

where r , c_p, k are the density, specific heat and thermal conductivity, respectively. At the heating surface, $a_{abs} F \cdot \hat{n} = -\hat{n} \cdot (k \nabla T)$, where a_{abs} is the material's absorbency and $\hat{n}$ is a unit vector normal to the surface pointing to the solid. The heat flux due to the Gaussian laser power is expressed as

$$F = Q_{\max} \exp(-R_k R^2) \text{ and } Q_{\max} = P_{laser} R_k / p \tag{5}$$

where $Q_{\max}$ is the heat flux intensity of the laser beam, R is the distance to the laser beam center, R_k is the concentration coefficient, and P_{laser} is the laser power.

All the surfaces of workpiece subject to the convective heat flux that is $f = h(T - T_s)$, where h is the convective heat transfer coefficient, T is the surface temperature, and T_s is the surrounding temperature. The radiation heat flux is also considered at the heating surface that is $f_c = e s (T^4 - T_s^4)$, where e and s are emissivity and Stefan-Boltzmann constant, respectively.

In the mechanical analysis, Hooke's law was used for elastic deformation, and for the plastic-deformation state, the flow rule is

$$de_{ij} = dl \frac{\partial f}{\partial s_{ij}} \tag{6}$$

where e_{ij} is the strain tensor, s_{ij} is the stress tensor, dl is the instantaneous, positive, varing, proportionality factor (plastic compliance), and $f = f(s_{ij})$ is the yield function. For anisotropic analysis Hill's potential function is applied instead of Von Mises function. Hill's yield criterion [12] can be written as

$$(G+H)s_{11}^2 - 2Hs_{11}s_{22} + (H+F)s_{22}^2 + 2Nt_{12}^2 = 1 \tag{7}$$

In a simple tension test performed in the rolling direction in the plane of the sheet, the incremental strain ratio can be written as

$$de_{11} : de_{22} : de_{33} = (G+H) : (-H) : (-G) \tag{8}$$

According to the definition of R-value (Eq. 3), it is obtained

$$\frac{H}{G} = \frac{de_{22}}{de_{33}} = R_0 . \tag{9}$$

Similarly, for a simple tension test performed in the 90^0 and 45^0 to the rolling direction,

$$\frac{H}{F} = R_{90} \quad \text{and} \quad \frac{N}{G} = (\tfrac{1}{2} + R_{45})(1 + \frac{R_0}{R_{45}}) \tag{10}$$

Since the thermal and mechanical deformations are symmetric about the vertical plane containing the scanning path, only half of the plate is modeled in the numerical simulation. In numerical simulation, the main assumptions used are as follows. Plastic deformation generated heat is small as compared to energy input in laser forming so that it is negligible. During the entire laser forming process, no melting takes place. The symmetric plane is assumed to be adiabatic. ABAQUS was used to complement the numerical simulation. The same mesh model was used for the thermal and mechanical deformations.

2.3 Results and discussions

2.3.1 Texture characterization

Fig.2a shows the four incomplete pole figures {100}, {110}, {111} and {112} of the cold-rolled steel sheet with thickness of 1.4 mm. The main texture components can be obtained from pole figures qualitatively. In the normal direction (*ND*), a stronger component of {111} and weaker components of {001} and {112} were seen. In the rolling direction (*RD*), a stronger <110> direction and weaker <001> and <112> directions were identified. Three major components of textures {111}<110>, {112}<110> and {001}<110> were therefore determined, while in the subsequent orientation distribution function (ODF) plots more exact components were obtained.

Fig.2b shows ODF sections (with j_2 increments from 0^o to 85^o) for the same material by EBSD. By transforming Euler angles to texture representation (*hkl*)[*uvw*], the major components of textures can be determined. The a -fiber textures are (112)[$1\bar{1}0$] and (001)[$1\bar{1}0$] and the g -fiber textures are (111)[$0\bar{1}1$] and (111)[$\bar{1}\bar{1}2$]. This observation is consistent with the texture development theory (Section 2a). That is, in lower reduction like this case (thickness of 1.4mm), {001}<110> and {112}<110> are the dominant components on the a -fiber (<110>//RD) and one sees a weak preference of {111}<112> on the g -fiber ({111}//ND). {111}<110> is dominant because it belongs to both a -fiber and g -fiber.

Fig.3a shows the {100},{110},{111} and {112} pole figures obtained from steel sheet 0.89 mm thick which represents larger rolling reduction. The obvious difference can be found in {100} pole figure compared with that of 1.4 mm steel sheet. {001} texture has disappeared and <110> is the major direction along the rolling direction. From ODFs on Fig.3b, the major components of textures are determined as a -fiber (112)[$1\bar{1}0$] to (111)[$1\bar{1}0$] and g -fiber (111)[$0\bar{1}1$]. The change of texture components is consistent to the texture development theory. That is, when

rolling reduction is higher, the maximum on the α -fiber is shifted to {112}<110> so that {001}<110> components can be neglected. In γ -fiber the components of textures shift from {111}<112> to {111}<110>.

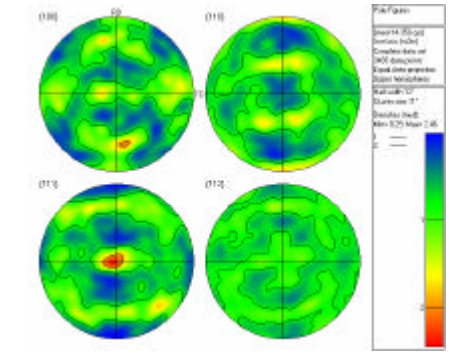

(a)

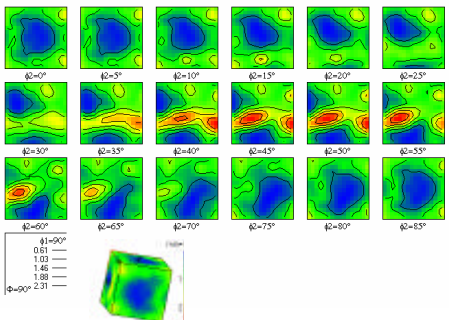

(b)

Fig.2 (a) Pole figures of AISI 1010 cold-rolled steel sheet 1.4 mm thick; and (b) orientation distribution functions (ODF) of the same sample

2.3.2 Macro anisotropic properties

Fig.4 shows *R*-values determined in tensile tests for two different sheet reductions and along three different angles to rolling direction. The pattern of *R*-values between the two reduction levels is somewhat similar but different in the following way. In the lower reduction case (thickness of 1.4mm), the *R*-value along the rolling direction (RD), R_0, is larger than that along the transverse direction (TD), R_{90}. While in the higher reduction case (thickness of 0.89mm), R_0 is slightly smaller than R_{90}. This result is consistent with theoretical predictions.

The prediction of *R*-values using the series expansion method is generally carried out within the framework of the Taylor's model[13]. To improve the accuracy of predictions, " Relaxed Constraint" grain interaction models are employed[14]. The Taylor or full constraint (FC) model had been shown to be more accurate in prediction at lower reduction cases. While in higher reduction cases, the relaxed constraint (RC) model is more accurate due to the more accurate boundary conditions.

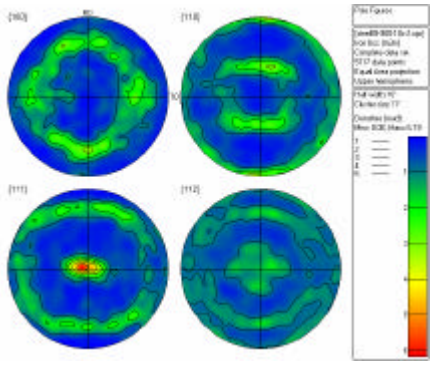

(a)

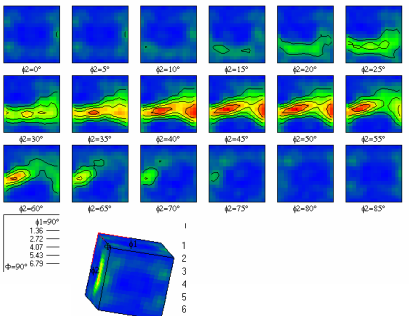

(b)

Fig.3 (a) Pole figures of AISI 1010 cold-rolled steel sheet 0.89 mm thick; and (b) orientation distribution functions (ODF) of the same sample.

From Fig.4, a very good agreement can be seen for the lower reduction case (thickness =1.4mm), while in Fig.6b agreement is again seen for R_0 and R_{90} but some discrepancy between the measured and predicated values is seen for R_{45}. A likely reason for the discrepancy is as follows. It is known that the RC approach is appropriate for describing the deformation of aggregates of pancake-shaped grains. For cold-rolled low carbon steel, the elongated flattened grains are mostly along the rolling direction. As a result, the predictions obtained from the RC model fit the experimental data somewhat better from 0 deg to 45 deg. For angles above 45 deg, the grains are no longer elongated along the tensile axis, so that the grain shape argument for using this model is not valid any more.

Fig. 4 also compares yield stress ratio between indirectly measured values and theoretical predictions. The measured-values are obtained by measured *R*-values and Hill's yield criterion . As expected, the prediction based on the FC model fits the lower reduction case closely and that based on the RC model fits the high reduction case closely.

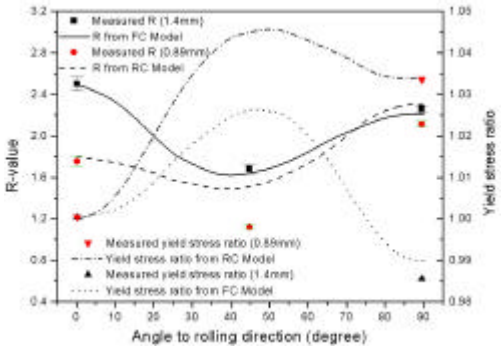

Fig.4 Comparison of *R*-values and yield stress ratio between measured value and theoretical prediction (Daniel and Jonas, 1990) for sheet metal of 1.4 mm thick and 0.89 mm thick

2.3.3 Anisotropic effect on laser forming involving different material reductions

80 by 80 by 1.4 mm samples were scanned along either *RD* or *TD*. Fig.5a shows the experimental and numerical results of bending angles caused by the laser scanning and a reasonable agreement is seen. There is an obvious difference in bending angle between scanning along *RD* and *TD*. Since the flow stress in *TD* is smaller than that in *RD* (Fig. 4), the bending angle when scanned along *TD* is smaller than that when scanned along *RD* because it is well known that the plastic deformation perpendicular to the scanning direction is primarily responsible for the bending angle.

To further illustrate the point, Fig.5b compares the simulated *y*-plastic strain (*y* is perpendicular to the scanning direction as shown in Fig. 1b) for scanning along *RD* and *TD*. As expected, it is smaller when scanned along *TD* than that along *RD*. Scanning on the same but hypothetically isotropic material is also superposed for comparison. The isotropic material is assumed to have *R*-values equal to 1 and the yield stress is 30% smaller than that of cold rolled sheet. The *y*-plastic strain of isotropic material is larger due to the smaller flow stress than that of the anisotropic material.

The bending angle difference of samples with thickness of 0.89 mm is quite different from that of samples with thickness of 1.4 mm. Since in this case the flow stress in *RD* is smaller than that of *TD* (Fig. 4), bending angle is smaller when scanning along *RD* than that of scanning along *TD*. This is consistent experimentally and numerically as shown in Fig .6.

In summery, difference of bending deformation exists when scanning along different directions in the anisotropic material used in this study. With the rolling reduction of steel sheet increasing, the anisotropic effect on laser induced bending is more pronounced. Anisotropic effect on laser forming under different heating conditions were also investigated. The detail can be found in Cheng and Yao[18].

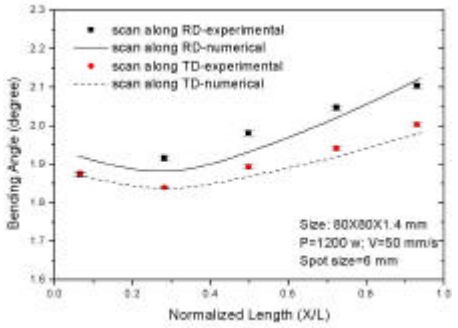

(a)

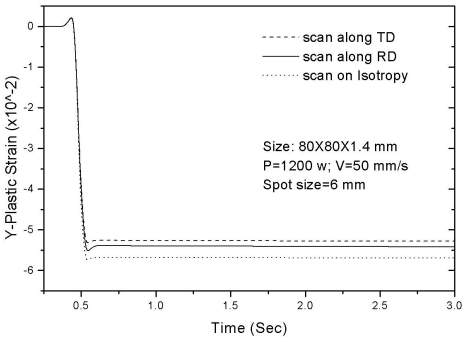

(b)

Fig.5(a) Numerical and experimental bending angles of 1.4mm thick steel sheet with scanning along *RD* and *TD*, respectively; (b) Simulated time history of plastic strain in the *y* direction, which is perpendicular to the scanning path (results on isotropic sheets also included).

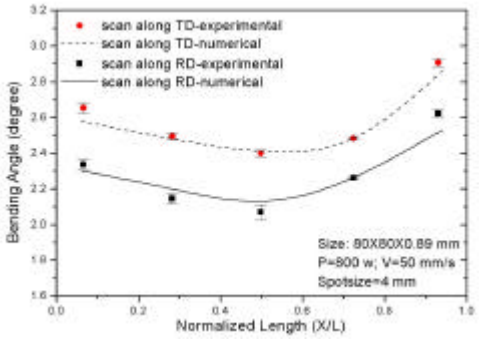

Fig.6 Numerical and experimental bending angles of 0.89mm thick steel sheet with scanning along *RD* and *TD*, respectively

3. Size effect on laser forming

3.1 Experiments and simulations

Experiments of straight-line laser forming (Fig.7) were carried out with the sheet length and width varying from 80 mm to 200 mm, in which the size effect was investigated in three cases: varying sheet width, varying sheet length, and varying square size. Additional set of samples (L = 20~60 mm, W = 80 mm) was also used to further investigate the

sheet length effect because it was reported[5] that the effect of sheet length is more pronounced when length-to-thickness ratio (L/s_0) is small. The sheet thickness is fixed at 0.89 mm since effect of thickness has been well studied as discussed in the previous section.

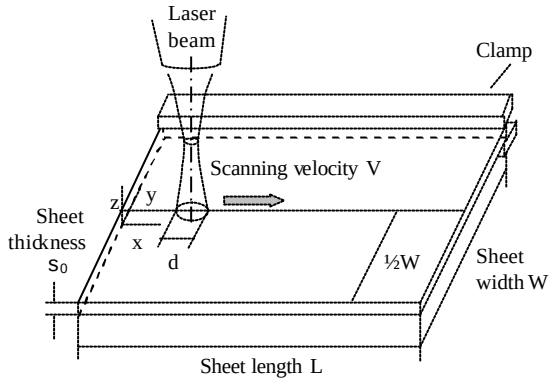

Fig.7 Schematic of straight-line laser bending.

3.1.1 Effect of sheet width

Fig.8 shows the variation of bending angle with the sheet width, length or both varying. It is seen from that, for low carbon steel, when the sheet width increases, bending angle decreases. This differs from the observation on LF of Inconel 625 [7], where it was reported that bending angle increases with both sheet width and sheet length and it was attributed to larger thermal stress caused by larger constraint from the cold plate. The discrepancy is indicative that the size effect on bending angle may not be as simple as it was proposed.

When the sheet width varies, both thermal conduction condition and sheet weight vary. In numerical simulation, the weight effect was removed by deleting the gravity term in the model. Fig.9 shows the bending angle difference between models with or without considering the gravity. It is found that, for the sheet width range investigated, the bending angle difference caused by gravity is almost the same for 80x80 and 80x200 samples, which clearly indicates that the gravity effect is not the major reason for the bending angles change caused by sheet width change. Further evidence was obtained by examining the Z-direction stress at a typical point and it is found that gravity does not affect the bending stress significantly even the sheet width increases from 80 to 200mm. So the reason of bending angle difference caused by different width may lie in the thermal conduction condition.

Fig. 10 shows the simulated time history of temperature. It is seen that the peak temperature at the top surface of workpiece drops when the sheet width increases, while the temperature at the bottom surface is almost the same. The reduced temperature gradient in the thickness direction is clearly responsible for the reduced bending angle when sheet width increases. This is obviously due to the fact that a larger width provides a larger heat sink.

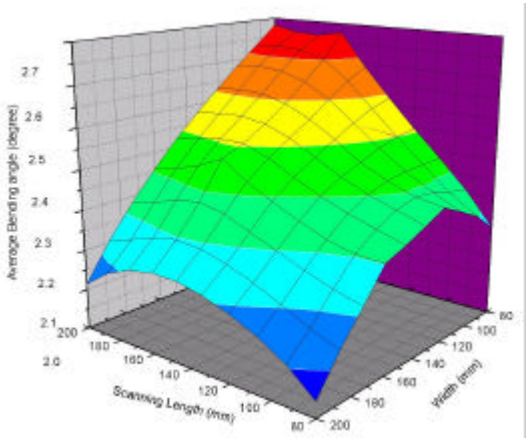

Fig.8 Average bending angle influenced by size effect.

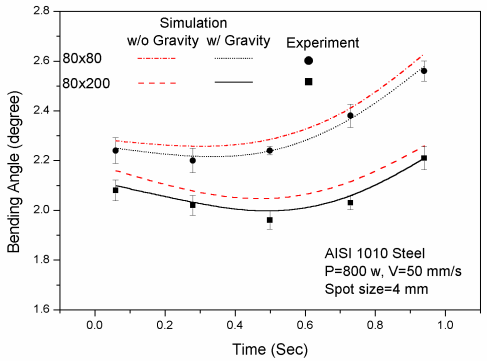

Fig.9 Influence of gravity of gravity on bending angle when the sheet width varies.

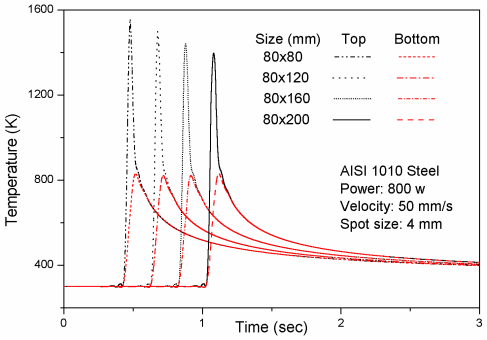

Fig.10 Simulated time history of temperature for different sheet width (0.2 seconds time delay between each case for viewing clarity).

3.1.2. Effect of Sheet Length

It is found that although the sheet length increases, the thermal field is not visibly affected. This is primarily

because the heat sink effect discussed above is over shadowed in the direction of sheet length by the fast moving laser beam along the same direction.

Fig.11 shows the time history of bending angle, peak temperature, and Z-direction stress in a 200x80 size sample at a typical position (x = 61.3 mm). It is seen that before the laser beam reaches that point (signified by the rapid rise of temperature), the bending angle has reached about 1/3 of the final bending angle. When the laser beam reaches that point, the bending angle increases rapidly approximately until the Z-direction stress stabilizes. The bending angle continues to rise slowly after the laser passes to the point. The existence of the pre-bending (bending at a location generated before the heat source arrives at the location) and post-bending (bending at a location generated after the heat source passes the location) obviously plays an important role in creating the final bending angle. It is also found that there is more pre-bending effect in the shorter sheet (80x80) than in the longer sheet (200x80), and the opposite can be said about the post-bending effect. In any case, within the sheet length range investigated, the pre-bending effect is more significant than the post-bending effect.

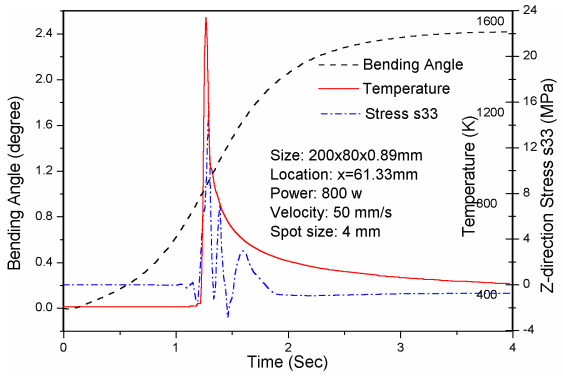

Fig.11 Simulated time history of bending angle temperature and stress.

3.1.3. Varying square sizes

It is seen in Fig.8 that for the varying square sizes, the bending angle increases before it decreases. This is clearly because of the competing effects of heat sink primarily associated with sheet width and the pre-/post-bending effect primarily associated with sheet length. The pre-/post-bending effect is more dominant initially and as a result the bending angle increases before heat sink effect takes over and thus the bending angle decreases.

3.2. Predictive model development

To predict size effect on laser forming, an analytical was developed to facilitate size effect prediction. The model is based on the solution to a moving strip heat source over a finite size sheet and on the account for pre-bending effect among consecutive segments on the scanning path. The detail derivation can be seen in Cheng and Yao[19].

Based on Rosenthal's moving heat source solutions, the analytical thermal model is developed with finite width condition and moving strip source considered. The temperature increment is

$$\Delta T = \frac{q}{r c_p a g V d}\left[\frac{1}{2lV} + \left(\frac{d}{2} - x\right) - \frac{e^{-2lV(d/2+x)}}{2lV} + \sum \frac{2}{m_n(m_n+1)} \cdot \frac{1-e^{-(m_n+1)lV(d/2+x)}}{lV} \cos\frac{npy}{a} + \sum \frac{2}{m_n(m_n-1)} \cdot \frac{1-e^{(m_n-1)lV(x-d/2)}}{lV} \cos\frac{npy}{a}\right] \quad (11)$$

Considering the pre-bending effect, the analytical mechanical model is developed based on two layer model. The derived bending angle is

$$\overline{a} = \left(1 - \frac{1}{3n}\right)\frac{2l_h}{s_0} a_{th} \Delta T \quad (12)$$

where

$$l_h \approx 0.125(P/V) + 0.5 \quad (13)$$

$$L/n \approx 3(P/V) - 17.5 \quad (14)$$

Above equation predicts the bending angle of a finite sized sheet. The effect of sheet width is reflected in ΔT and the effect of sheet length is reflected in n. The unit of length, power and velocity is mm, watt and mm/s, respectively.

3.3. Validation of the predictive model

Figs. 12 and 13 show the validation of the proposed model. It is seen that the bending angle values obtained from the proposed model show a similar trend as the experiments and simulation, while the existing analytic model is unable to predict the size effect. Although the proposed model over estimates the bending angle, its agreement with experimental and simulation values is significantly better compared with the other analytical model. The main reason for this over estimate comes from the omission of yield strength consideration in the proposed analytical model. The fraction of the heat energy absorbed by the zones, where the heated temperature is below the critical temperature to effect appreciable plastic deformation, is almost 25% of the total input energy[5], while the model assumes all the input energy is used for deformation.

In the case of varying sheet length, the model predicted trend of bending angle is well agreeable with the experimental and simulation values. The trend is consistent with Vollertsen's[5] experimental observations, that is, when the ratio of length and thickness is small, the increasing trend of bending angle with sheet length is more pronounced and there is an upper limit of bending angle when the sheet length keeps increasing. In the comparison of varying square size, the predictive model also captures the variation trend.

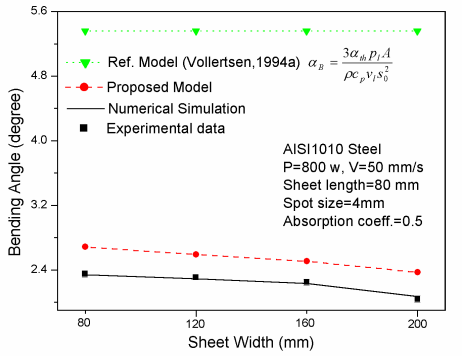

Fig.12 Analytic prediction of bending angle for varying sheet width

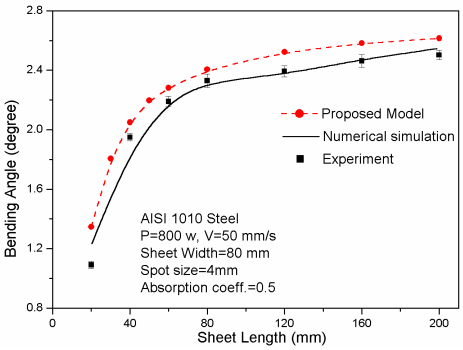

Fig.13 Analytic prediction of bending angle for varying sheet length

4. Conclusions

The effects of plastic anisotropy and size effect on laser forming were experimentally and numerically investigated. The anisotropic effect increases with the rolling reduction. If scanning velocity increases while laser power is kept constant, the anisotropic effect increases relative to the bending deformation, primarily due to shorter time and lower temperature for recrystallization. If the scanning velocity is kept constant while laser power increases, higher temperature will make the anisotropic effect smaller relative to the deformation. In multi-scan laser forming process, repeated recrystallization during multiple scanning and different increment of flow stress in RD and TD will reduces the anisotropic effect.

Within the sheet size range as well as process condition used in this investigation, the size effect on laser forming of low carbon steel sheet can be summarized as follows. When sheet length is constant and sheet width increases, the bending angle slightly decreases. This is primarily due to the increased heat sink effect with sheet width. When sheet width is constant and sheet length increases, the bending angle slightly increases. This is primarily due to the fact that the bending angle along the scanning path is non-uniform and influenced by the pre-/post-bending effect. When both the sheet length and sheet width increase as square sheets, the bending angle increases before decreases due to the competing effects. Based on the experimental and numerical results and physical interpretations above, an analytical model is developed to predict the size effect. The analytic model compares favorably with the existing analytical model in terms of agreement with experimental measurement and numerical simulation.

Acknowledgements

This work is supported by NSF grant (DMI-0000081) and a NIST ATP grant (#00005269). Support from Columbia University is also gratefully acknowledged.

References

[1] Kuwabara, T., and Ikeda, S., " Plane-strain Tension Test of Steel Sheet using Servo-controlled Biaxial Tensile Testing Machine," *J. Mater. Processing Technology*, Vol. 80-81, 1998: 517-523

[2] Liao, K. C., Friedman, P. A., Pan, J., and Tang, S. C., "Texture Development and Plastic Anisotropy of B.C.C. Strain Hardening Sheet Metals," *Int. J. Solids Structures*, Vol. 35, No.36, 1998: 5205-5236

[3] Scully, K., " Laser Line Heating," *Journal of Ship Production*, Vol. 3, No. 4, 1987: 237-246

[4] Koloman, K., and Kraol, P., "Formen durch locale Erwarmung," *Metal Forming-Theory and Practice: Proceedings of the 5th International Conference on Metal Forming*, Tisza, M., and Kardos, K. (Eds), 1991: 69-75

[5] Vollertsen, F., " An Analytical Model for Laser Bending," *Lasers in Engineering*, Vol. 2, 1994: 261-276

[6] Vollertsen, F., " Mechanisms and Models for Laser Forming," *Laser Assisted Net Shape Engineering, Proceedings of the LANE'94*, Vol. 1, Meisenbach Bamberg, 1994: 345-360

[7] Hsiao, Y. C., Maher, W., et al., " Finite Element Modeling of Laser Forming," *Proc. ICALEO'97*, Section A, 1997: 31-40

[8] Kocks, W. K., Tome, C. N., and Wenk, H. R., *Texture and Anisotropy-preferred orientations in polystals and their effects on materials properties*, Cambridge University Press, London, 1998

[9] Raabe, D., and Lucke, K., " Rolling and Annealing Textures of BCC Metals," *Materials Science Forum*, Vol. 157-162, 1994: 597-610

[10] Hosford, W. F., and Caddell, R. M., *Metal Forming-Mechanics and Metallurgy (2nd Ed.)*, Prentice-Hall International, Inc., London, 1993

[11] Taylor, G. I., "Plastic Strain in Metals," *J. Inst. Metals*, Vol. 62, 1938: 307-324

[12] Hill, R., " A Theory of the Yielding and Plastic Flow of Anisotropic Metals," *Proceedings of the Royal Society of London, Series A, Mathematical and Physical Sciences*, Vol. 193, Issue 1033, 1948: 281

[13] Bunge, H. J., *Texture Analysis in Materials Science-Mathematical Method*, Butterworths, London, 1982

[14] Daniel, D., and Jonas, J. J., " Measurement and Prediction of Plastic Anisotropy in Deep-Drawing Steels," *Metallurgical Transactions A*, Vol. 21A, 1990: 331-343
[16] Masubuchi, K., " Studies at MIT Related to Applications of Laser Technologies to Metal Fabrication," *Proc. of LAMP'92*, 1992: 939-946
[17] Rosenthal, D., " The Theory of Moving Sources of Heat and Its Applications to Metal Treatments," *Transactions of the ASME, Journal of heat transfer*, Vol. 68, 1947: 849-866
[18] Cheng, P, and Yao, Y. L, " The Influence of Sheet Metal Anisotropy on Laser Forming Process," *Proceedings of the ICALEO'03*, Section E, 2003:1-10
[19] Cheng, P, and Yao, Y. L, " Analysis and Prediction of Size Effect on Laser Forming of Sheet Metal," submitted to *Journal of Manufacturing Process.*

Contact info:
Y. Lawrence Yao
Professor
Department of Mechanical Engineering
Columbia University
220 Mudd Bldg., MC 4703
New York, NY 10027, USA
Tel: 212-854-2887, Fax: 212-854-3304
Email: yly1@columbia.edu